AIP | Journal of Applied Physics

In situ studies of the crystallization kinetics in Sb–Ge films

Amanda K. PetfordLong, R. C. Doole, C. N. Afonso, and J. Solís

Citation: J. Appl. Phys. **77**, 607 (1995); doi: 10.1063/1.359045

View online: http://dx.doi.org/10.1063/1.359045

View Table of Contents: http://jap.aip.org/resource/1/JAPIAU/v77/i2

Published by the American Institute of Physics.

In situ studies of the crystallization kinetics in Sb–Ge films

Amanda K. Petford-Long[a] and R. C. Doole
Department of Materials, University of Oxford, Parks Road, Oxford OX1 3PH, United Kingdom

C. N. Afonso and J. Solís
Instituto de Optica, CSIC, Serrano 121, 28006 Madrid, Spain

(Received 3 February 1994; accepted for publication 29 September 1994)

The crystallization process in Sb_xGe_{1-x} alloy films has been observed during *in situ* annealing in a transmission electron microscope. Results are presented for two films with $x=0.89$ (89 at. % Sb) and $x=0.71$ (71 at. % Sb), which lie on either side of the eutectic composition ($x=0.85$). In the former films radial crystals are observed to grow rapidly from discrete nuclei, whereas in the latter films the crystallization process occurs through a near-planar front. In addition, quantitative data obtained from these experiments show that the $Sb_{0.89}Ge_{0.11}$ films have a higher activation energy for crystal growth and a lower temperature for the nucleation of crystals. Significant differences are observed between the crystallization processes for the two films studied, with the $Sb_{0.89}Ge_{0.11}$ film showing better potential for development as an ultrafast optical phase-change storage medium. © *1995 American Institute of Physics.*

I. INTRODUCTION

A precise knowledge of the crystallization kinetics of thin films is of great importance for the development of suitable phase-change erasable optical storage media. Phase-change optical storage technology takes advantage of the difference in optical properties between amorphous and crystalline phases and to make it competitive, crystallization has to be achieved with short, even ultrashort, laser pulses.[1,2] Therefore the time needed for crystal nucleation and growth needs to be minimized.

Several multicomponent media have been proposed which typically involve chalcogenides and/or antimony: GeTe,[3] SbSe,[4] InSbTe,[5] GeTeSb,[6] Sb–O,[7] and GeSb.[2,7] Several works have reported results on the crystallization kinetics of optical storage media,[4,8,9] with diffusionless transformations being found to lead to shorter transformation times.[3,4] It has also been proposed that crystallization speed depends on the incubation time (time for which film has been heated prior to the onset of crystallization) rather than on the activation energy,[8] and that the stability of the amorphous phase is enhanced when large activation energies for crystallization are involved.[4,9] It has recently been demonstrated that crystallization can be induced in Sb-rich GeSb alloys by means of short[2,10] and ultrashort[2,7] laser pulses. The crystallization time of Sb_xGe_{1-x} alloys under 250 ns pulses is found to depend strongly on the composition of the films, with films on either side of the eutectic composition showing very different properties.[10] The higher Sb-content films were found to exhibit both the largest change in optical reflectivity upon crystallization and the shortest crystallization times.

The aim of this work is to study the kinetics of the crystallization process in SbGe films. The films have been crystallized by isothermal treatments during *in situ* observation in a transmission electron microscope (TEM), and the crystallization process recorded on video tape for subsequent quantitative analysis. Two films were chosen for *in situ* analysis, with compositions of $Sb_{0.89}Ge_{0.11}$ and $Sb_{0.71}Ge_{0.29}$, which are above, and below, the eutectic composition (85 at. % Sb), respectively. The two films studied have optical properties, and show a behavior under laser irradiation, which are representative of other films with compositions above and below the eutectic composition.[10] The former films have a higher activation energy for crystal growth and a lower crystal nucleation temperature. The crystallization process in the $Sb_{0.89}Ge_{0.11}$ is interface-controlled and occurs with an almost constant nucleation rate.

II. EXPERIMENTAL DETAILS

A. Specimen preparation

A series of amorphous alloy films, approximately 50 nm thick, were grown at room temperature in a dc magnetron sputtering system, onto carbon-coated mica substrates. The films were grown by codeposition from Ge and Sb (99.999% purity) targets. The deposition rate for Ge was 0.3 nm s^{-1} and two different deposition rates (2.0 and 0.8 nm s^{-1}) were used for Sb in order to obtain $Sb_{0.89}Ge_{0.11}$ and $Sb_{0.71}Ge_{0.29}$ films. The background pressure was 3×10^{-6} mbar and the operating pressure of argon was 5×10^{-3} mbar.

TEM specimens were made by floating the SbGe films off the mica substrate onto distilled water, and picking them up on copper TEM grids. The films were then analyzed in plan view (i.e., with the electron beam parallel to the film normal).

B. Annealing

The specimens were observed during *in situ* heating in a JEOL 4000EX TEM (point-to-point resolution limit of 0.25 nm), and the temperatures were measured with an integral thermocouple mounted in the furnace body. The microscope column vacuum was approximately 3×10^{-7} mbar. Each specimen was held at approximately 100 °C *in situ* for at least 20 min to allow it to stabilize and to outgas any water vapor or other contaminants, thus preventing them from be-

[a]E-mail: amanda.petford-long@materials.ox.ac.uk

ing deposited on the specimen surface during annealing. The specimens were heated from 100 °C to their anneal temperatures at a rate of the order of a few degrees Kelvin per second. A range of annealing temperatures were used, between 192 and 216 °C for the $Sb_{0.89}Ge_{0.11}$ films and between 260 and 328 °C for the $Sb_{0.71}Ge_{0.29}$ films.

Crystallization of the as-grown films was followed in the dark field (DF) imaging mode using an objective aperture to select part of the innermost amorphous ring from the as-grown film. On crystallization, the electrons passing through the film will be diffracted either into, or out of, the objective aperture, resulting in a change of contrast for all crystalline regions, irrespective of crystallographic orientation. Some of them will appear darker than the surrounding amorphous film, and others brighter. In measuring the crystallized fraction from each video frame, both darker and brighter areas are taken into account. The contrast between amorphous and crystalline regions is higher in the DF mode than that in the bright field mode, making observation of the crystallization front movement easier to follow, and increasing the accuracy of subsequent measurements. After crystallization has started, it is possible to select a diffracted spot for conventional DF imaging and thus image each radial grain in turn. The experiments were recorded onto video tape, using a TV/image pickup system, along with a time code to enable accurate recognition of individual video frames. Diffraction patterns and images were also recorded onto photographic film.

C. Determination of crystallization kinetics

The crystallization kinetics of amorphous metallic alloys under isothermal conditions is usually described by the phenomenological Avrami equation[11]

$$x = 1 - \exp(-kt^n),$$

where x is the crystalline fraction at time t, k a kinetic parameter which depends on temperature, and the exponent n is determined by the transformation mode and can easily be determined by plotting $\ln[-\ln(1-x)]$ vs $\ln(t)$. The exponent n is usually partitioned as follows:

$$n = a + bp,$$

where $0<a<1$ refers to the nucleation rate and b to the dimensionality of the crystal growth, having values from 1 to 3. p defines the mechanism which controls growth and is equal to 0.5 for diffusion-controlled transfer and equal to 1.0 for an interface-controlled process.

The crystallized fraction and the position of the crystallization front were measured from the video recordings. Individual video frames were digitized for subsequent processing. Since the experiments were carried out using a PAL video system, the time interval between consecutive video frames is fixed at 40 ms. The magnification of both the video recording and the frame store were calibrated by recording an image of a magnification calibration standard on both devices.

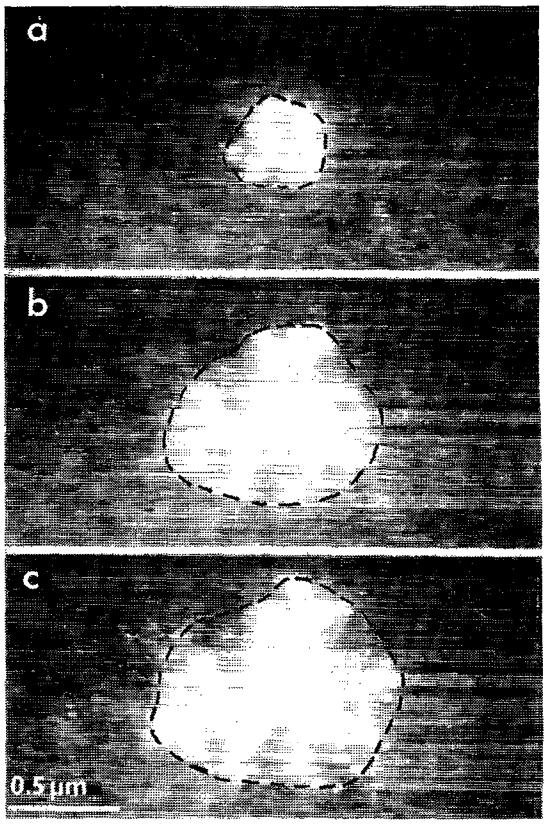

FIG. 1. Sequence of three DF images of an $Sb_{0.89}Ge_{0.11}$ film recorded during *in situ* annealing, showing the typical growth of a radial crystal. The time separation between consecutive images is 0.16 s.

D. Postannealing analysis

The annealed specimens were analyzed further at room temperature. HREM analysis was carried out using another JEOL 4000EX TEM (point-to-point resolution=0.16 nm) to obtain atomic-scale information about the crystallographic structure of the films, and microdiffraction was carried out using a JEOL 2010 TEM to identify the crystal type and crystallographic orientation of the grains. In order to determine the distribution of the constituents in the crystallized films, a VG HB501 field-emission gun scanning TEM (FEG STEM) equipped with an energy dispersive x-ray (EDX) spectrometer was used. X-ray spectra were recorded at each point of matrix of up to 512×512 points, and the corrected Sb and Ge peak integrals were used to produce elemental distribution maps of the area being analyzed. The VG HB501 was used because of its high spatial resolution (2 nm). Further chemical analysis was carried out using EDX analysis in the 2010 TEM.

III. RESULTS

A. $Sb_{0.89}Ge_{0.11}$ films

Figure 1 shows three DF images of the same region of the $Sb_{0.89}Ge_{0.11}$ film, recorded from a video sequence during *in situ* crystallization in the TEM. Small disk-shaped crystals were observed to nucleate at several positions across the

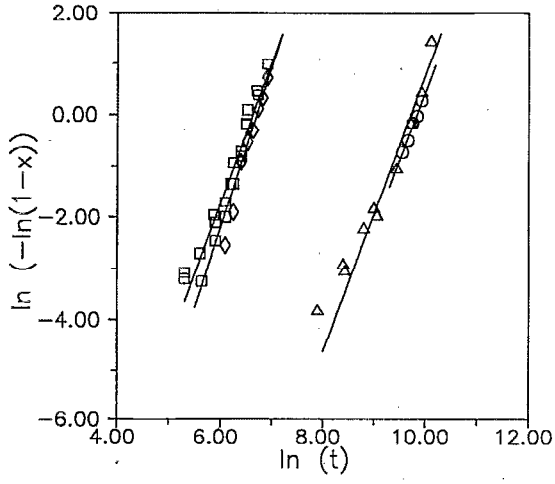

FIG. 2. Crystallized fraction (x) of $Sb_{0.89}Ge_{0.11}$ films, plotted as $\ln[-\ln(1-x)]$ vs $\ln(t)$. Results obtained at 217, (□), 210 (◇), 200 (△), and 192 °C (○) are included.

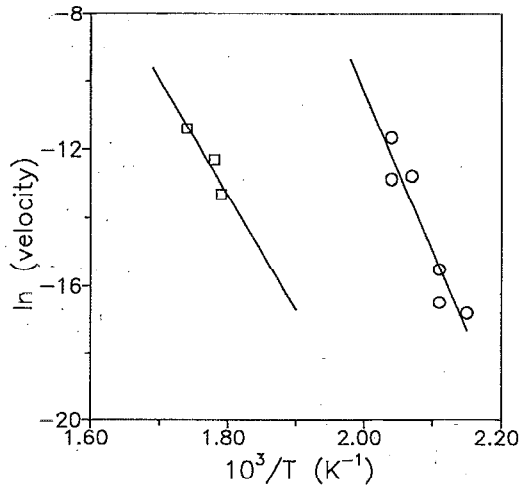

FIG. 3. Arrhenius plot of the crystal front velocity to determine the activation energy for crystal growth. Results obtained from the $Sb_{0.89}Ge_{0.11}$ film (○) and the $Sb_{0.71}Ge_{0.29}$ film (□) are both included.

film, and to grow radially as crystallization proceeded, for all annealing temperatures studied. From images similar to those in Fig. 1, the crystallized fraction at different times could be measured, as described in Sec. II C above. The time at which crystallization initiates (the time origin) was taken as the first video frame at which contrast could be observed from the crystal nuclei. Because of the low contrast and small size of the nuclei, our time origin could be one or two video frames (40 or 80 ms) later than the real start of the crystallization process. For the same reason, crystal fractions lower than 10%–12% are subject to a greater error than the higher crystal fractions.

The data could be well fitted to the Avrami equation via ln vs ln plots, as shown in Fig. 2 for crystallized fractions higher than 10%–12%, with the average slope leading to a transformation index of $n=2.9(\pm 0.3)$. The growth velocities were calculated by measuring the mean diameter of the disk-like crystals as a function of time. The velocities were in the range 10^{-8}–10^{-6} ms^{-1} and could be used to determine an approximate value for the crystal-growth activation energy[12] from an Arrhenius plot as shown in Fig. 3. The slope yields an activation energy of 4.0 eV.

Figure 4(a) shows a DF image of a fully crystallized $Sb_{0.89}Ge_{0.11}$ film, annealed *in situ* at 210 °C. The associated selected area diffraction (SAD) pattern obtained from the central bright grain is shown in Fig. 4(b), and a diagram indicating the indexing of the diffraction spots is shown in Fig. 4(c) with an SAD pattern from the as-grown film shown in Fig. 4(d) for comparison. The other bright regions are different radial grains with the same crystallographic orientation as that from which the diffraction pattern in Fig. 4(b) was recorded. The dark regions are radial grains with crystallographic orientation such that their diffracted spots lie outside the aperture used to form the particular image seen in Fig. 4(a). On heating, the radial grains increased in size until they contacted with other grains, resulting in faceted and irregular shapes as opposed to the initial disk shape. A single radial grain consists of many crystals, the majority of which have the same, or a very similar, crystallographic orientation. At the slower crystallization rates, we observed grains overlapping other radial grains as they grew. Since the radial grain size is one or two orders of magnitude larger than the film thickness, this result shows that crystallization nucleates in more than one plane of the specimen.

At all the annealing temperatures analyzed, the entire $Sb_{0.89}Ge_{0.11}$ film crystallized with a strong fiber texture, namely $[00.1]_{Sb}$ and $\langle 111\rangle_{Ge}$ parallel to the film normal. Figure 4(b), recorded from a single radial grain, shows that for this radial grain, in addition to the strong fiber texture, there is a three-dimensional orientation relationship between the Ge and Sb crystals, observed at all anneal temperatures, with the $\{11\bar{2}0\}_{Sb}$ planes parallel to the $\{220\}_{Ge}$ planes. The same orientation relationship between the Sb and Ge crystals was observed for all the radial grains.

A typical HREM image of a region within a radial grain of the $Sb_{0.89}Ge_{0.11}$ film, crystallized at 200 °C, is shown in Fig. 5. This shows that the single-crystal regions within the radial grains are of the order of 20–30 nm. Lattice fringes with a hexagonal symmetry are visible, with the majority of crystals being Sb. This result was confirmed by the analysis of chemical composition maps, and by the use of nanobeam electron diffraction (NBD), using a 10 nm incident probe, to record electron-diffraction patterns from individual crystals within the radial grains. The chemical composition map shown in Fig. 6 indicates, in addition, preferential segregation of Ge to the radial grain boundaries following crystallization. A smaller amount of Ge is distributed throughout the radial grains, this Ge being in crystalline form, as shown by the use of NBD.

B. $Sb_{0.71}Ge_{0.29}$ films

The crystallization process of the $Sb_{0.71}Ge_{0.29}$ films is very different from that described above for the $Sb_{0.89}Ge_{0.11}$

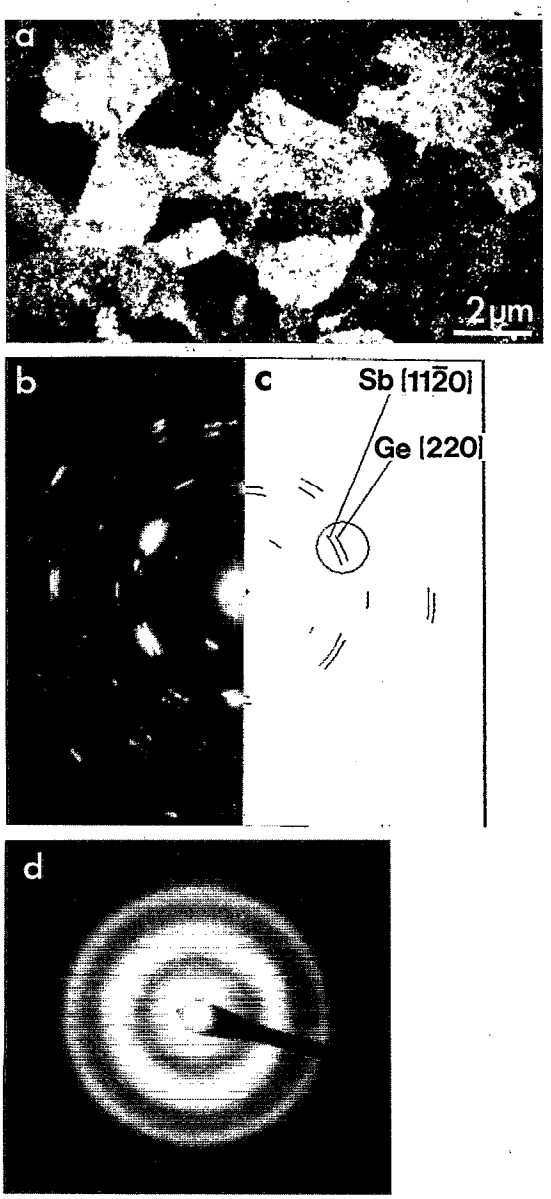

FIG. 4. (a) DF image of a fully crystallized $Sb_{0.89}Ge_{0.11}$ film after annealing at 210 °C with (b) the corresponding SAD pattern from the central bright radial grain. (c) Schematic of the SAD pattern shown in (b). The Bragg spots used to form the DF image in (a) are indicated. The inner arc corresponds to the $\langle 11\bar{2}0\rangle$ Sb lattice spacing and the outer arc to the $\langle 220\rangle$ Ge lattice spacing. (d) SAD pattern of the as-grown film.

films. Crystals are now nucleated at, or close to, the TEM support grid bars and the crystallization front proceeded by small crystals forming ahead of the main crystallization front, with the areas "behind" these crystals crystallizing later, as can be seen in Fig. 7(a). This resulted in a crystallization front within each grid square which moved towards the center of the square, until the entire region was crystalline.

With the film held at constant temperature, the motion of the front was observed to slow down with time, until no further crystallization occurred. As an example, at an anneal

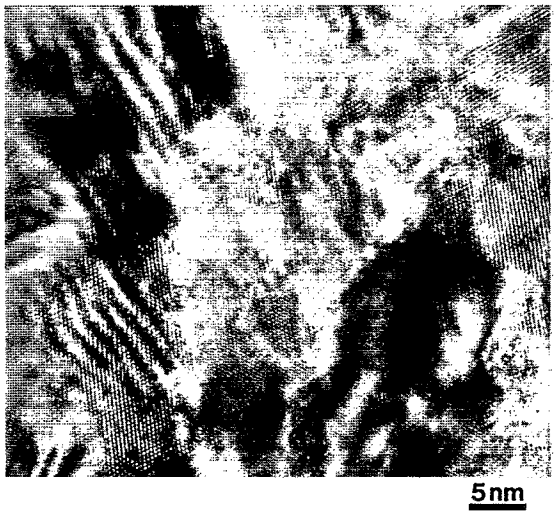

FIG. 5. Typical HREM image showing crystals within a radial grain of a fully crystallized $Sb_{0.89}Ge_{0.11}$ film after annealing at 200 °C.

temperature of 290 °C, it took 35 min for the crystallization front to stop moving and even after this time there was a substantial portion of each grid square in which the film was still amorphous. As the crystallization rate decreased, the crystallization front became wider and more uneven, eventually becoming of the order of 1 μm wide. The fact that the crystallization rate decreased with time at a constant anneal temperature made it very difficult to obtain reliable data for the crystallization fractions. For the same reason, the crystal-growth velocities were measured immediately following initial nucleation in order to get an accurate comparison between anneals carried out at different temperatures. These results have also been included in Fig. 3 and yield an activation energy for crystal growth of 2.9 eV.

With the specimen held at constant temperature, an increase in crystal size with time from approximately 100 to

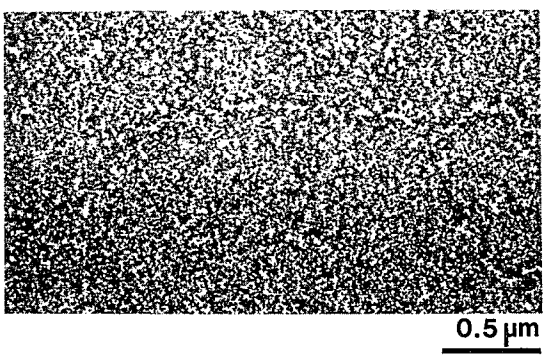

FIG. 6. STEM EDX composition map of a fully crystallized $Sb_{0.89}Ge_{0.11}$ film showing segregation of Ge to edges of radial grains. The bright regions of the image indicate a high Ge content.

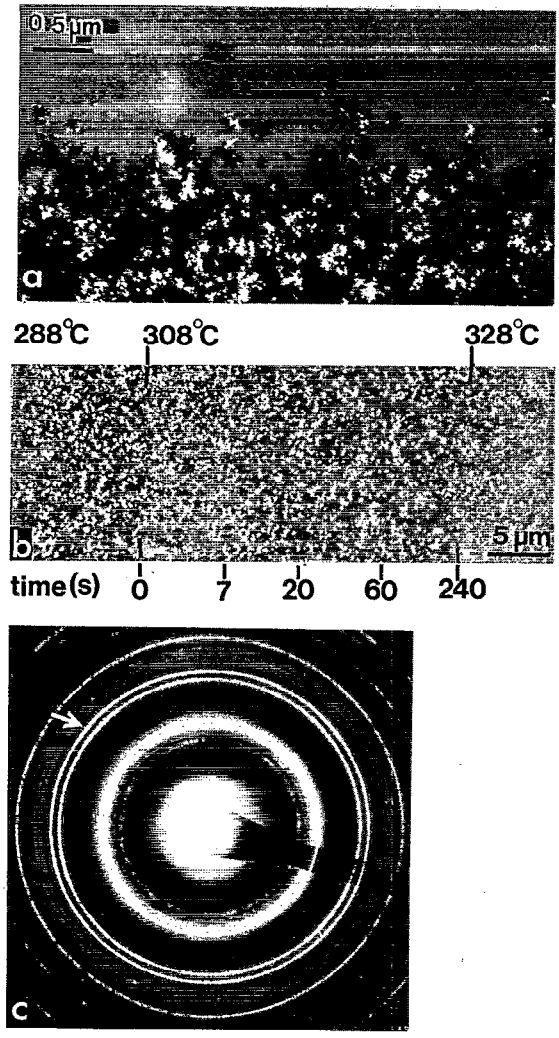

FIG. 7. (a) DF image of the crystallization front of the $Sb_{0.71}Ge_{0.29}$ film following annealing to 270 °C. (b) DF image of a film held constant at each of three successive temperatures of 288, 308, and 328 °C. It can be seen that the grain size increases with time at each constant temperature. The position of the crystallization front with time, at 308 °C, is indicated. (c) Diffraction pattern from fully crystallized film.

approximately 500 nm occurred, at the same time as the decrease in crystallization front velocity. If the temperature was then increased, crystallization continued more rapidly, with an associated decrease in crystal size. The change in crystal size can be seen in Fig. 7(b), on which the extent of crystallization nucleated at three increasing temperatures is indicated. Initially the temperature was held constant at 288 °C. At $t=0$ the temperature was increased rapidly to 308 °C and then held constant. On initially increasing the temperature, the crystal front velocity increased, with small grains being formed. As time continued at 308 °C, the velocity gradually decreased, with a consequent increase in the size of grains formed. At $t=240$ s the temperature was again increased, to 328 °C. This resulted in another increase in crystal front velocity with an associated decrease in grain size. Higher crystallization rates resulted in smaller crystals, which contrasts with the $Sb_{0.89}Ge_{0.11}$ films, for which similar

FIG. 8. Typical HREM image of $Sb_{0.71}Ge_{0.29}$ film after crystallization, showing the random orientation of the crystalline grains.

crystal sizes were observed independent of rate. The diffraction patterns from areas of the film with a low crystallization rate showed spotty rings, while diffraction patterns from areas of the specimens with a higher rate of crystallization showed smoother rings, confirming this result.

Diffraction patterns recorded from the crystallized $Sb_{0.71}Ge_{0.29}$ film showed that both Ge and Sb crystals were present, but no preferred growth orientation was observed. This result was further confirmed by the HREM images, an example of which is shown in Fig. 8, taken from a region of a film crystallized at 284 °C. The image was recorded close to a grid bar, at which crystallization nucleated, and thus shows the early stages of crystallization. The crystals are not very uniform in size, and no clear orientation relationship or crystal texture can be seen. EDX analysis of the crystallized film showed that the distribution of Ge and Sb atoms is irregular, with no evidence of preferential segregation. However, EDX analysis of crystals ahead of the main crystallization front (for a film which had been cooled to room temperature before it had completely crystallized) suggested that the earliest crystals to nucleate are Sb or Sb-rich.

IV. DISCUSSION

The crystal nucleation and growth processes for SbGe films are very different for films with composition on either side of the eutectic composition. The crystallization temperatures obtained in the work presented here are in very good agreement with those reported earlier for films grown by thermal evaporation.[13] Although the crystal morphology observed in the $Sb_{0.71}Ge_{0.29}$ films also agrees quite well with earlier observations, that of the $Sb_{0.89}Ge_{0.11}$ films is very different, as described above. The formation of both Sb and Ge crystals in the two films is also in very good agreement with the phase diagram of the GeSb system[14] which predicts a 6 at. % solid solubility of Ge in Sb under equilibrium conditions, which is in contrast to the value of >17 at. % reported under quenching experiments.[14,15] Since the GeSb system has no stable phases, concentrations of Ge higher than 6%

should lead to phase separation as observed experimentally.

The discussion of the crystallization kinetics will be centered on the $Sb_{0.89}Ge_{0.11}$ films, since this is the most attractive film for development for optical storage applications,[2,10] in addition to being the film for which more information concerning the crystallization process could be obtained. The discussion will be completed with some comments regarding the crystallization kinetics of the $Sb_{0.71}Ge_{0.29}$ film and an evaluation of the crystallization kinetics, determined in the films with compositions on either side of the eutectic, for optical storage applications.

The crystallization process in the $Sb_{0.89}Ge_{0.11}$ films involves an initial transient period during which a number of small crystals nucleate across the film. As crystallization proceeds, we observe the nucleation of new crystals at the same time as the growth of other crystals, the number of new nuclei forming decreasing slowly with time. The very earliest stage of nucleation cannot easily be seen because of the low contrast which it displays in the TEM, and so the role of incubation times in the crystallization kinetics,[8] and an activation energy for nucleation, could not be determined. Note that the radial grains grow so fast that it is not possible to analyze the nuclei using HREM, because of the drift of the image as the temperature is increased. HREM has, however, been used successfully to follow the much slower processes occurring at the grain boundaries in Sb/Ge layered films from the very earliest stages of the reactions.[16] At the highest temperatures studied, the rapid growth rate made it very difficult to measure the rate of appearance of new crystal nuclei during the crystallization process, and thus to assess whether the rate decreased with time.

The crystallization appeared to nucleate at more than one level within the film thickness since the DF images have shown how two radial grain images can overlap while growing. This was confirmed by halting the crystallization process for one specimen as soon as the DF image showed any crystalline contrast. At this stage of the process, the SAD pattern showed weak spots with clear evidence still of the halos observed in the SAD patterns of the as-grown amorphous films, showing that only partial crystallization of the films had occurred. These halos gradually disappeared as the film crystallized through its thickness, to give a fully crystallized material. Further evidence for this could be seen in the DF images, which showed a continued increase in crystalline contrast following nucleation, as the film crystallized through its thickness. Most of the initial nucleation sites are expected to be at the film surface with crystallization progressing across the surface(s) of the film before proceeding through the film thickness. Our results are consistent with a mixed process involving bulk nucleation in addition to surface nucleation, suggesting the presence of both homogeneous and heterogeneous nucleation.

The analysis of the crystallized fraction in the frame of the Avrami theory for crystallization leads to a transformation index $n(=a+pb)=2.9(\pm 0.3)$. Since the TEM images show clearly that crystals grow radially and therefore the growth process is two dimensional, the above transformation index is consistent with an interfacially controlled growth with a nearly constant nucleation rate (or one which slightly decreases with time). This conclusion is further supported by the fact that the growth rate is found experimentally to be approximately constant at a given temperature, in contrast with the parabolic dependence expected in the case of a diffusion-controlled process.

The crystallization process in the $Sb_{0.71}Ge_{0.29}$ film is quite different from that described above for the $Sb_{0.89}Ge_{0.11}$ films. Nucleation of crystals is observed to start at, or close to, the bars of the Cu support grid. Once crystallization has started, preferential nucleation sites exist on a fine scale across the crystallization front. Two possible explanations for this result are, first, since the grid bars are in thermal contact with the furnace body, they may be slightly hotter than the rest of the film, resulting in a thermal gradient which acts as a driving force for crystal nucleation. Second, crystallization may be nucleated at the grid bars simply because the film is in contact with the grid, and is therefore under different stress or surface energy conditions than the free-standing film over the grid squares. These facts suggest that nucleation is predominantly heterogeneous.

The fact that the crystal front velocity is found to decrease with time is consistent with a diffusion-controlled process which could also be driven by the initial thermal gradient mentioned above, or by stresses at the grid bar. The random-successive-nucleation model used to explain fractal formation in GeAl[17] can be also used to analyze the front movement in our case. Once crystal nuclei are formed, the heat released can lead to a local temperature rise adjacent to the front. Since thermal diffusion is faster than atomic diffusion, the heat flow can stimulate new nuclei appearing in the nearby regions, as we observe experimentally.

The activation energy for crystal growth is found to be higher for the $Sb_{0.89}Ge_{0.11}$ film than for the $Sb_{0.71}Ge_{0.29}$ film. This result is not unexpected since it has usually been reported that a large activation energy and transformation index n indicate rapid crystallization of amorphous materials[8] and the former films have indeed shown shorter crystallization times.[10] In addition, large activation energies are necessary to enhance the stability of the amorphous phase,[9] which is a necessary requirement for developing suitable phase-change media for optical recording. The present results show that, although the initial crystal-growth velocity is similar for both the film compositions analyzed, the $Sb_{0.89}Ge_{0.11}$ films are fully crystallized within seconds whereas the crystallization process in the $Sb_{0.71}Ge_{0.29}$ films stops, typically after several tens of minutes, without fully crystallizing the film. This is a consequence of the different crystallization mechanisms, an interface- versus a diffusion-controlled process, which makes $Sb_{0.89}Ge_{0.11}$ films good candidates as fast crystallizing materials for optical storage applications.

The fact that Sb crystals with a very strong crystalline texture are produced in the $Sb_{0.89}Ge_{0.11}$ films, as opposed to the randomly oriented crystals formed in the $Sb_{0.71}Ge_{0.29}$ films, may also contribute to the higher optical contrast observed in the former films. The strong crystalline texture developed in the $Sb_{0.89}Ge_{0.11}$ films following crystallization is very similar to the crystal structure and texture observed in crystalline films of pure Sb. The fact that this strong texture does not appear in the $Sb_{0.71}Ge_{0.29}$ films could be related to

the higher Ge content which prevents its solution into the Sb lattice, thus promoting the segregation of randomly oriented crystals.

V. CONCLUSIONS

The hypereutectic films (in this study, $Sb_{0.89}Ge_{0.11}$), richer in Sb than the eutectic composition, are found to crystallize fast through an interface-controlled process with a near constant nucleation rate. The activation energy for crystal growth is quite high (~4.0 eV), which ensures the stability of the amorphous phase. In contrast, the hypoeutectic films (in this study, $Sb_{0.71}Ge_{0.29}$), with a composition on the other side of the eutectic composition, crystallize through a diffusion-controlled process with a growth velocity which rapidly slows down with time. These results show that only films with an Sb content higher than that of the eutectic have crystallization kinetics consistent with the requirements for optical storage applications.

ACKNOWLEDGMENTS

This work has been partially supported by CICYT under the TIC93-0125 project. We are grateful to The British Council/Spanish Joint Research Program for traveling finances, the Glasstone Benefaction (AKPL), Professor R. J. Brook for provision of laboratory facilities, and the Materials Modelling Laboratory at Oxford for computing facilities. Dr. Neil Long is thanked for operation of the FEG STEM and production of the composition map shown in Fig. 6.

[1] K. A. Rubien, Mater. Res. Soc. Symp. Proc. **230**, 239 (1992).
[2] C. N. Afonso, J. Solís, F. Catalina, and C. Kalpouzos, Appl. Phys. Lett. **60**, 3123 (1992).
[3] M. Chen, K. A. Rubin, and R. W. Barton, Appl. Phys. Lett. **49**, 502 (1986).
[4] H. Situ, Z. T. Wang, and A. Jung, J. Non-Cryst. Solids **113**, 88 (1989).
[5] Y. Maeda, I. Ikuta, H. Andoh, and Y. Sato, Jpn. J. Appl. Phys. **31**, 451 (1992).
[6] N. Yamada, E. Ohno, K. Nishiuchi, N. Akahira, and M. Takao, J. Appl. Phys. **69**, 2849 (1991).
[7] C. N. Afonso, M. C. Morilla, J. Solís, N. H. Rizvi, M. A. Ollacarizqueta, and F. Catalina, Mater. Sci. Eng. A **173**, 343 (1993).
[8] Y. Sugiyama, R. Chiba, S. Fujimori, and N. Funakoshi, J. Non-Cryst. Solids **122**, 83 (1990).
[9] M. Okuda, J. C. Rhee, J. Fusong, H. Naito, and T. Matsushita, Jpn. J. Appl. Phys. **26**, 26 (1987).
[10] J. Solís, C. N. Afonso, J. F. Trull, and M. C. Morilla, J. Appl. Phys. **75**, 7788 (1994).
[11] P. Altuzar and R. Valenzuela, Mater. Lett. **11**, 101 (1991); S. Ranganathan and M. Von Heimendahl, J. Mater. Sci. **16**, 2401 (1981).
[12] J. L. Batstone, Philos. Mag. A **67**, 51 (1993).
[13] T. Okabe, S. Endo, and S. Saito, J. Non-Cryst. Solids **117/118**, 222 (1990).
[14] B. C. Giessen and C. Borromee-Gautier, J. Solid State Chem. **4**, 447 (1972).
[15] R. Serna, C. N. Afonso, F. Catalina, A. K. Petford-Long, N. Teixeira, M. F. da Silva, and J. C. Soares, Nucl. Instrum. Methods B **64**, 807 (1992).
[16] A. K. Petford-Long, R. C. Doole, C. N. Afonso, and F. Catalina, Proc. ICEM **13** (Paris), 463 (1994).
[17] L. Bo-Quan, Z. Bin, Z. Shy-Yuan, and W. Zi-Qin, Phys. Rev. B **47**, 3638 (1993).